Development of Dual Phase Steel for LPBF Applications

Kerri Horvay, Christopher Schade and Thomas Murphy
Hoeganaes Corporation
Cinnaminson, NJ

ABSTRACT

As additive manufacturing (AM) expands into the structural and automotive parts market more suitable materials need to become available that are tailored to these applications. For this study, a dual phase (DP) steel was chosen because of its combination of high strength and ductility. Its microstructure typically consists of two phases: islands of hard martensite and a soft ferrite matrix. Currently, DP steels are used in various automotive components that are produced by conventional manufacturing methods. The mechanical properties of laser powder bed fusion (LPBF) test specimens are evaluated as well as heat treated properties to show the range of properties that can be developed with a single alloy system. This provides greater flexibility to the end user by allowing one material to be utilized in a range of applications. Microstructures and porosity are evaluated for gas atomized powder and discussed in relation to the build parameters and the mechanical properties.

INTRODUCTION

Currently, there is a need for more materials to be qualified for use in different additive manufacturing processes. Thus, it is important to explore new material possibilities by investigating the potential of existing wrought alloys currently being used for serial production parts. Dual phase steels are widely used in the automotive market and are processed by traditional thermomechanical methods. This steel can be found in wheel rims as well as safety critical car components.[1] As compared with conventional steels, DP steels have superior formability which is beneficial to part fabrication, particularly in stamped autobody panels.

Components made from DP sheet metal are created from steel slabs that may go through various hot and cold rolling processes to reduce its thickness. Then the steel sheet is passed through a continuous annealing furnace at a high temperature to intercritically anneal into the ferrite-austenite region.[1] It is cooled rapidly to transform the austenite to typically 20% of a hard second phase (martensite) surrounded by a soft ferrite matrix. This results in a microstructure that provides high strength, good ductility, and a

low yield strength (YS) to ultimate tensile strength (UTS) ratio.[2,3] Higher elongations at similar ultimate tensile strengths can be reached with DP steels as compared with conventional steels.[2]

Alternatively, parts manufactured by LPBF are created by sweeping metal powder across a build platform, then rapidly melting and cooling the powder layer by layer. Gas atomization produces spherical powder for this AM process that enhances bed packing, spreading and flow to achieve high density.[2] The raw materials are melted in an induction furnace prior to atomization and then inert gas impacts the molten steel, which solidifies into fine metal powder particles. Using LPBF with this steel is of interest due to the ability to produce parts with complex geometries. However, processing DP steel by LPBF uses a different thermal profile than conventional methods where the final microstructure is controlled by various factors such as the rolling processes, intercritical annealing temperature, time at temperature, and the cooling rate. To achieve similar properties to wrought, the laser melted DP steel part can also be intercritically annealed after printing to transform the microstructure to a desired mixture of ferrite and martensite. The wrought grade, DP600, was chosen for this study to evaluate the final properties achievable through LPBF processing. Because the intercritical annealing temperature and cooling rate influence the final transformation products, investigating the temperatures where these transformations occur is important in designing a heat treatment that will give specified properties for this alloy.

EXPERIMENTAL PROCEDURE

Powder Characterization

DP600 powder produced by gas atomization was screened to a nominal 20-63 µm particle size, which is common for LPBF processing. Scanning electron microscopy (SEM), using a JEOL 6460 LV SEM, was used to evaluate the powder morphology. Light optical metallographic (LOM) images of the etched powder particle cross-section were taken and microindentation hardness values were measured. Carbon, sulfur, oxygen and nitrogen content were measured by LECO analysis. Apparent density, tap density and flow were measured following MPIF standards 28, 46, and 03.[3] Particle size was measured using a Sympatec Helos BF laser-particle size analyzer following ASTM B822.

LPBF Processing

An EOS M290 AM machine with a building volume of 250 x 250 x 325 mm was used to make the specimens for this study by melting powder layer by layer with an Yb fiber laser (400W) within an argon filled chamber. Process settings can be varied to find the optimal energy density for the material being built. Equation 1 shows the formula for energy density where P is laser power (W), v is the scanning speed (mm/s), h is the hatch distance (mm), and t is the layer thickness (mm).

$$E = \frac{P}{v*h*t} \ , \left[\frac{J}{mm^3}\right] \quad (1)$$

Cubes samples (10 x 10 x 10 mm) were printed with a variety of different settings to evaluate the porosity content produced with the DP600 material. A constant layer thickness was used for all the samples while the laser power, hatch distance and scanning speed were changed. Image analysis was used to measure the porosity content of the cross-section of the cubes perpendicular to the build direction.

Dilatometry

A cylindrical sample was printed in the Z plane and cut from the build plate in the as-built condition. A high temperature dilatometer with nitrogen gas was used to heat the sample to 1050 °C and then was cooled at 0.27 °C/sec, which was calculated between 800 °C to 500 °C during cooling. Phase transformation temperatures were determined from a plot of temperature versus dilation.

Mechanical Testing

A set of standard settings was used to build the mechanical testing specimens (MPIF Standard 10 flat dogbone, flat axial fatigue, MPIF Standard 61 compressive yield strength) for this study.[3] Samples were cut from the build plate in the as-built condition after production. Tensile specimens were heated to various temperatures for 1 hr followed by air cooling. Axial fatigue specimens were tested as-built as well as after heat treating at 816 °C for 1 hr followed by water quenching. Hydraulic MTS machines, models 858 and 810, at a frequency of 40 Hz and fully reversed stress cycling (R= -1) were used. Survival to 2 x 10^6 cycles was considered a "run-out". Apparent hardness measurements were taken according to MPIF Standard 43. Compressive yield strength was tested in the as-built and intercritically annealed conditions. Standard metallographic techniques were used to evaulate the microstructure of the as-built and heat treated samples.

RESULTS & DISCUSSION

Powder Characterization

The chemical composition of the gas atomized powder used in this study is shown in Table I as well as the wrought specification for DP600. All of the measured alloying elements of the powder are within the maximum limits and the oxygen content is very low due to the inert gas used during atomization.

Table I. Chemical composition of powder used in this study and wrought DP600 (wt.%)

	C	O_2	Cr	Si	Mn	Fe
Powder	0.12	0.04	0.08	0.27	1.57	Bal.
Wrought	0.14 max	---	1.00 max	1.50 max	2.00 max	Bal.

Figure 1 shows the SEM micrographs of the powder and etched microstructure of a particle cross-section. The particles are very spherical with few satellites. This powder morphology is beneficial to the laser printing process because it leads to better flow during spreading and packing in the bed. The powder particle shown in Figure 1b has a very fine microstructure with an average microindentation hardness of 639 HV_{10}gf.

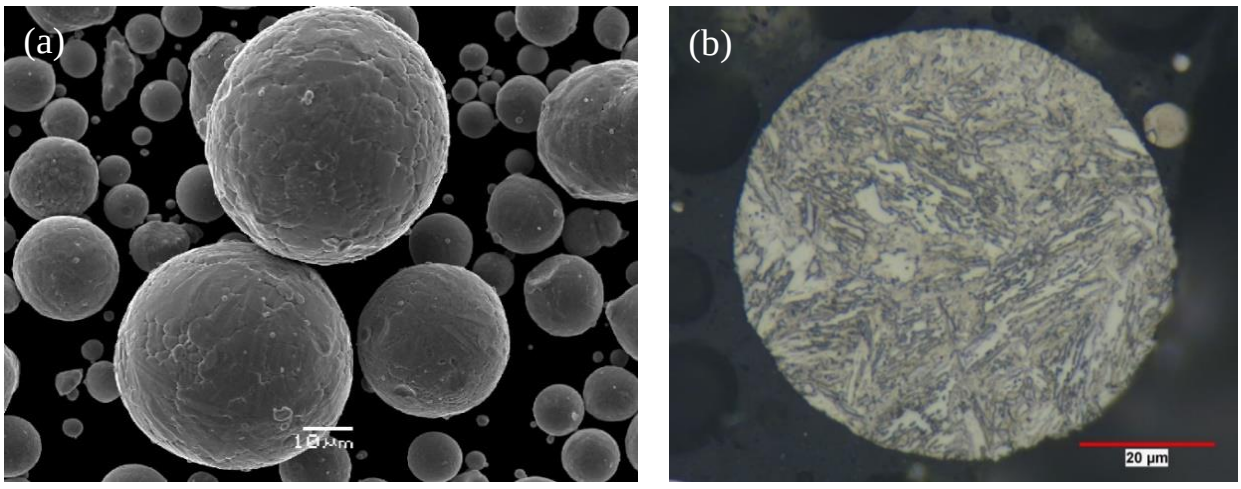

Figure 1. (a) SEM micrograph of the DP600 powder and (b) etched microstructure of cross-section of powder particle.

Table II shows measured properties of the powder including particle size, apparent density, tap density and flow measured with a carney funnel. The particle size was within the typical range used for LPBF processing. The density and flow measurements were also typical for gas atomized powders. Flowability

is an important factor for powders used in LPBF because the powders need to spread evenly across the build platform.

Table II. Powder properties

d_{10} [µm]	d_{50} [µm]	d_{90} [µm]	Apparent Density [g/cm^3]	Tap Density [g/cm^3]	Carney Flow [s/50g]
13	34	57	4.52	4.88	4

LPBF Parameter Optimization

Figure 2 shows the relative density measured by image analysis plotted against the applied energy density used to build the cubes. As the energy density increased the overall relative density of the cubes increased. A variety of settings produced almost full density samples of this material. The cubes showed a small amount of very fine porosity, but as the energy density increased the porosity was reduced. Cracking was also not observed in the cube samples, which is beneficial as compared with high strength steels that rely on higher carbon levels to provide strength that may produce cracks during printing.

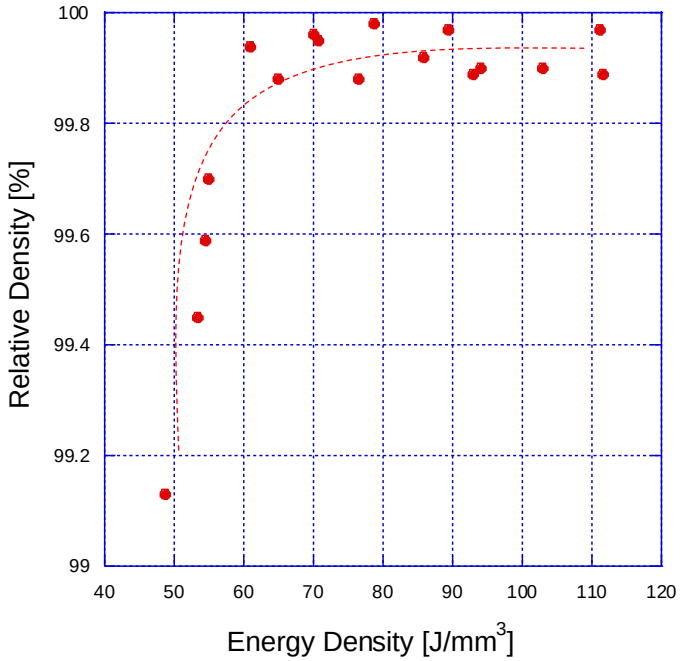

Figure 2. Relative density of the as-built cubes as a function of energy density.

SEM was used to analyze the microstructure of the as-built samples (Figure 3). It is difficult to discern the phases present due to the fine microstructure, but it appears to contain a mixture of martensite, bainite and ferrite. There is also some fine, rounded porosity that is visible and the grains appear angular. X-ray diffraction and electron backscattering diffraction could be used to verify what phases are in the microstructure.

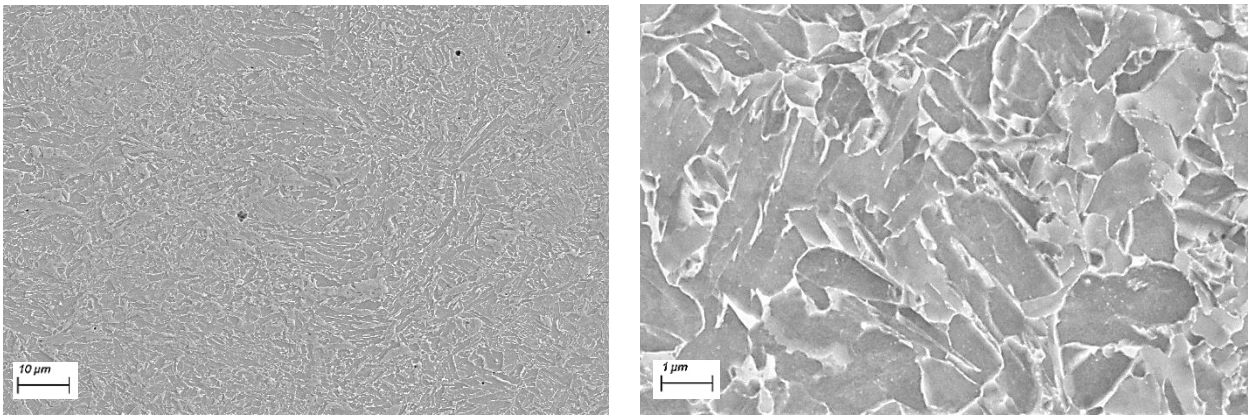

Figure 3. SEM micrographs of as-built sample at two different magnifications.

Figure 4 shows a phase diagram of DP600 grade steel by varying carbon content. The red dashed line shows the phases present at equilibrium at different temperatures for the alloy used in this study. The temperatures where the red line intersects the austenite and ferrite field is the intercritical annealing temperature range and is shown by the blue circles. By using the lever rule the amounts of austenite and ferrite at equilibrium can be calculated.[4] When the steel is heated in this temperature range and rapidly cooled the unstable austenite will transform to martensite or bainite and the ferrite will remain.

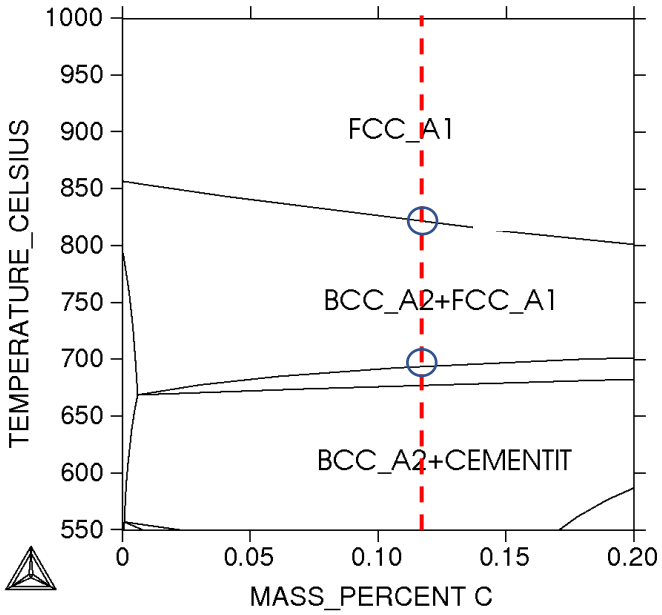

Figure 4. DP600 phase diagram

Dilatometry

Figure 5 shows the calculated Continuous Cooling Transformation (CCT) diagram for the DP600 material used in this study. This diagram indicates what phases transform at different cooling rates and is useful when considering different heat treatments. If the pearlite and bainite curves are missed by a fast enough cooling rate austenite will transform to martensite.[4] The starting grain size can affect how fast transformations happen due to changing the amount of surface area available for nucleation.[5] Thus, the CCT diagram for a wrought DP600 material will be different than a laser printed material due to the difference in starting grain size.

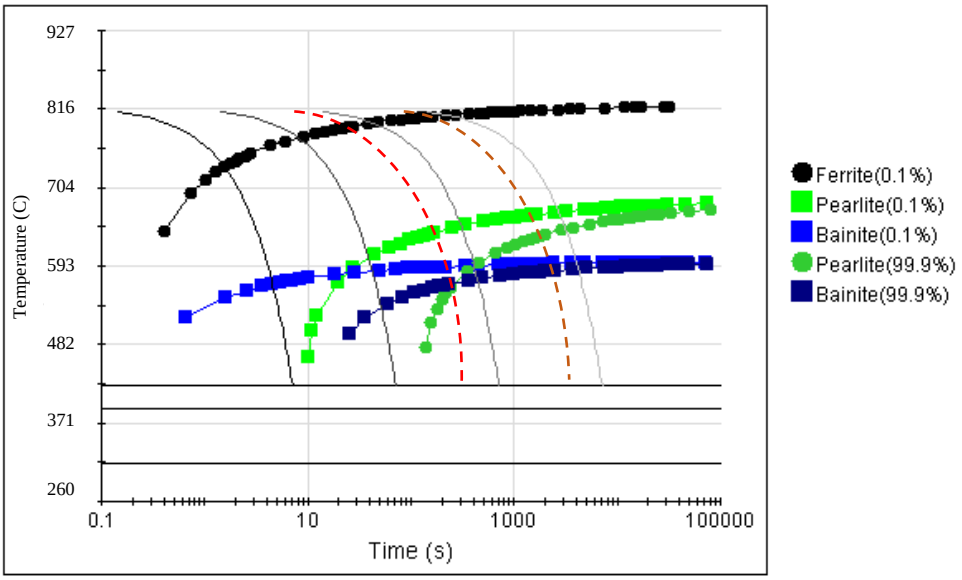

Figure 5. CCT diagram for DP600 alloy with starting grain size of 10 µm. The red line indicates the cooling rate of the air cooled samples. The orange line indicates the cooling rate used for the dilatometry test. Calculated using CALPHAD.

Figure 6 shows the dilatometry curve generated from an as-built sample and the heating profile. Dilatometry is a useful tool that can provide temperatures that phase transformations occur at by measuring volumetric changes of crystal structure during heating and cooling.[6] A change in slope indicates the start of a phase transformation.[7] The 1st derivative of the heat up and cool down portions of the dilatometer curve were used to estimate the Ac_1 (the lowest temperature that austenite can form) and the Ac_3 (the temperature that the austenite transformation finishes), 710 °C and 880 °C.[7] The ferrite start (F_s) and pearlite start (P_s) temperatures were estimated at 770 °C and 610 °C.

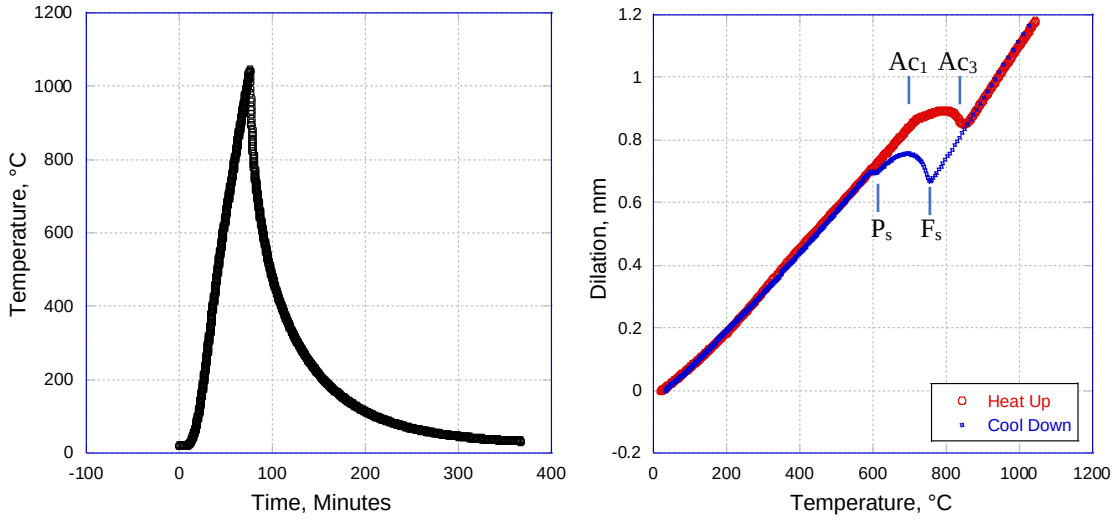

Figure 6. Graphs of temperature vs time and dilation vs temperature for DP600.

The microstructure of the dilatometer sample as shown in Figure 7 is fine with varying grain sizes that are becoming more uniform as compared with the as-built microstructure in Figure 3. The lighter areas appear to be ferrite and the darker areas appear to be pearlite.

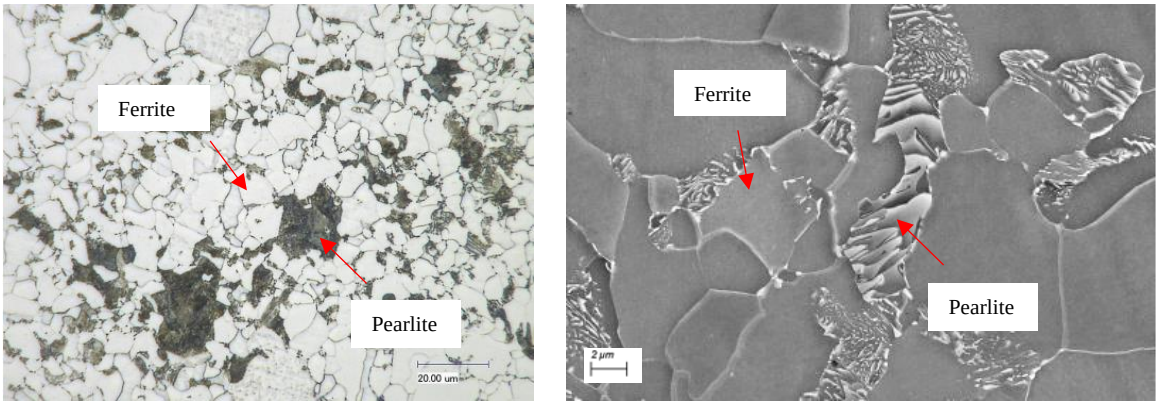

Figure 7. LOM and SEM micrographs showing microstructure of dilatometer sample.

Mechanical Properties

Table III shows the mechanical properties from heat treating the as-built tensile bars at various temperatures for 1 hr under a nitrogen atmosphere followed by air cooling. The as-built samples did not meet the wrought elongation requirement but exceeded the YS and UTS requirement. As the heat treating temperature increased the UTS and YS both decreased while the elongation increased. This trend changes at 760 °C where the YS and UTS begin to increase and the wrought specifications are met. From the dilatometry testing the Ac_1 temperature was estimated to be 710 °C, so the deviation we see in heat treated properties at 760 °C is within this intercritical annealing temperature range. When increasing the heat treating temperature to 816 °C and 871 °C the YS and UTS begin to decrease again and the wrought specifications are not met.

The as-built and tempered samples up to 538 °C had a high YS to UTS ratio while the intercritically annealed samples had a low ratio, which may be required by certain automotive part applications.[8] Heat treated laser printed parts with a high YS/UTS ratio may be desired for safety critical components and parts with a low YS/UTS ratio would be needed for components such as crumple zones.[8] By using different heat treating temperatures, times at temperature and cooling rates the mechancial properties of this alloy by LPBF can continue to be developed.

Table III. Mechanical properties of LPBF specimens

Condition	0.2%YS [MPa]	UTS [MPa]	Elongation [%]	Apparent Hardness [HRA]
Wrought (Salzgitter)	*330-470*	*580-670*	*>24.0*	---
As-Built	931	931	18.3	64
538 °C AC	752	772	20.3	60
649 °C AC	310	462	33.7	46
760 °C AC	455	579	32.0	53
816 °C AC	407	517	34.0	53
871 °C AC	393	503	35.3	49

The as-built microstructure appears fine and as the heat treatment temperature increases to 538 °C the structure becomes coarser as shown in Figure 8. At the 649 °C heat treatment temperature the grains are larger and the lighter areas appear to be ferrite. Assuming the as-built microstructure consists of mostly

martensite, when heating the samples below the Ac_1 temperature, 710 °C, the martensite will become tempered. The carbides will precipitate from the martensite until its carbon reduces and it becomes ferrite.[5] Grain growth will occur as the temperature increases causing the hardness to decrease.[5] The fine uniform features throughout the microstructure of the 649 °C heat treated sample appear to be spherical carbides dispersed in ferrite. Carbon has a lower solubility in ferrite than austenite due to the larger interstitial sites of the FCC crystal structure.[5] The 760 °C heat treated sample's microstructure is fine as compared with the 649 °C heat treated sample. At 760 °C, according to the phase diagram, there should be about 50% austenite at equilibrium which will nucleate differently depending on the starting structure. Assuming the starting microstructure is martensitic the austenite will then form at the carbide ferrite interface.[5]

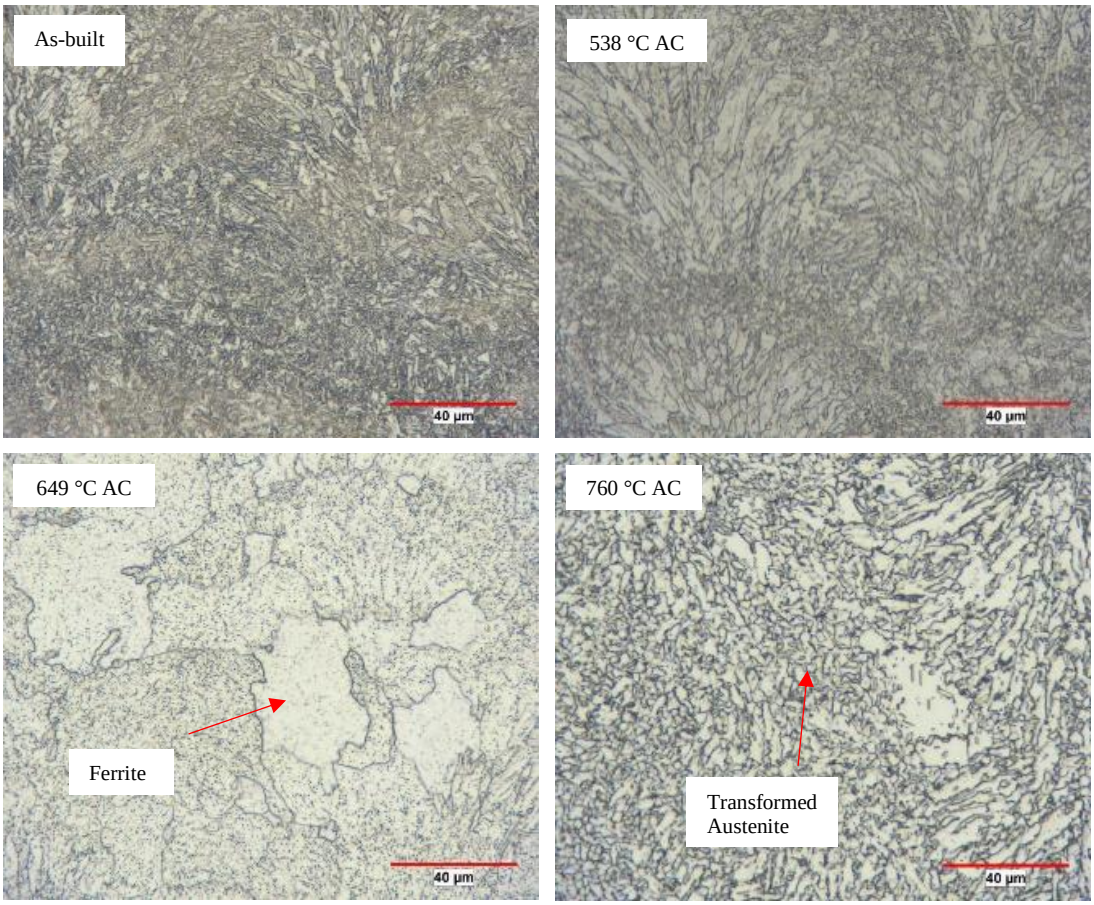

Figure 8. Etched microstructures of as-built and air cooled heat treated samples.

Compressive Yield Strength

Table IV shows the YS results for samples tested in both tension and compression. Samples were printed at different angles to investigate the effect of printing orientation. These as-built samples tested in tension and compression had similar YS's ranging from 910 to 958 MPa for the parts built at 0°, 30°, and 90° angles. Tension and compression samples were also intercritically annealed at 721°C for 1 hr and then water quenched. These samples resulted in a lower YS in compression than tension. This may be due to the volume expansion that occurs when austenite transforms to martensite upon rapid cooling, thereby inducing compressive residual stresses in the martensite.[2] This difference in yield strength in compression and tension is important to note depending on what the final application of the part may be.

Table IV. Mechanical properties of LPBF specimens

Test	Printing Orientation	Condition	YS, MPa
Tension	0°	As Built	931
Compression	0°	As Built	951
Compression	30°	As Built	910
Compression	90°	As Built	958
Tension	0°	721 °C WQ	269
Compression	90°	721 °C WQ	179

Figure 9 shows the etched microstructures of the compressive YS specimens intercritically annealed at 721 °C. Microindentation hardness measurements were taken in the light areas and dark areas. The lighter areas showed a hardness of 204 HV_{25}gf as compared with the darker areas with 380 HV_{25}gf. From these measurements the light areas are assumed to be soft ferrite and the darker areas containing a harder transformed austenite phase, most likely martensite.

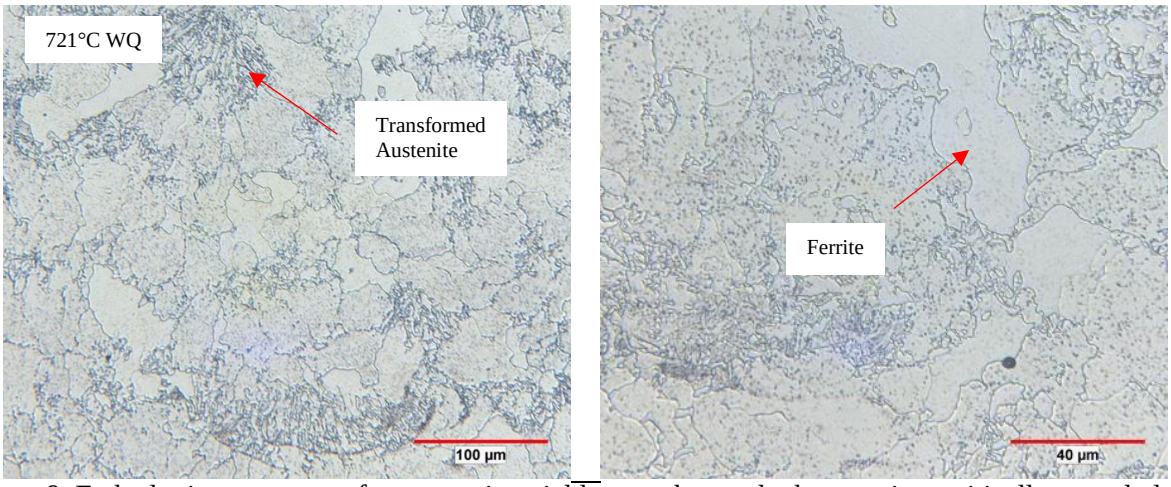

Figure 9. Etched microstructure of compressive yield strength sample that was intercritically annealed at 721 °C and water quenched showing two different magnifications.

Axial Fatigue Testing

İnvestigating fatigue performance is important for steels with automotive applications. The two fatigue curves in Figure 10 showed similar slopes however the as-built samples exhibited higher fatigue strength than the heat treated samples. Fatigue strength usually trends with ultimate tensile strength which supports the data because the as-built samples had a higher UTS as seen in Table III. The fatigue limit of a steel is estimated to be about half of the tensile strength.[1] A range of fatigue limits that trend with the UTS from the different heat treatments can then be assumed. For wrought DP600 using this estimation the fatigue strength would be 300 MPa, so the laser printed samples would have slightly lower fatigue strength in the as-built condition. Factors such as pores, grain size, and martensite content can affect the fatigue behavior, which is important because it limits its use in certain applications.[1]

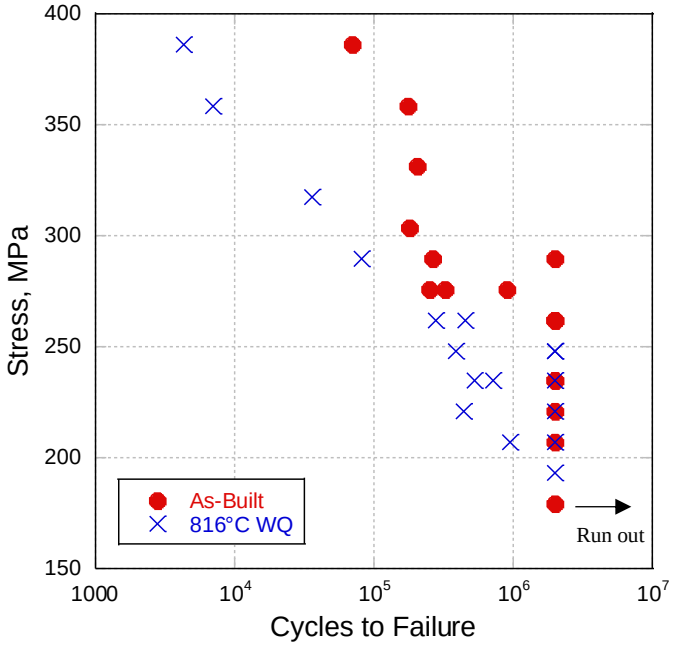

Figure 10. Axial fatigue response

There was a small amount of rounded porosity found in the fatigue samples as shown in Figure 11. The heat treated fatigue samples showed larger grains as well as some larger areas of ferrite which may have led to the lower fatigue strength as compared with the as-built samples (Figure 8).

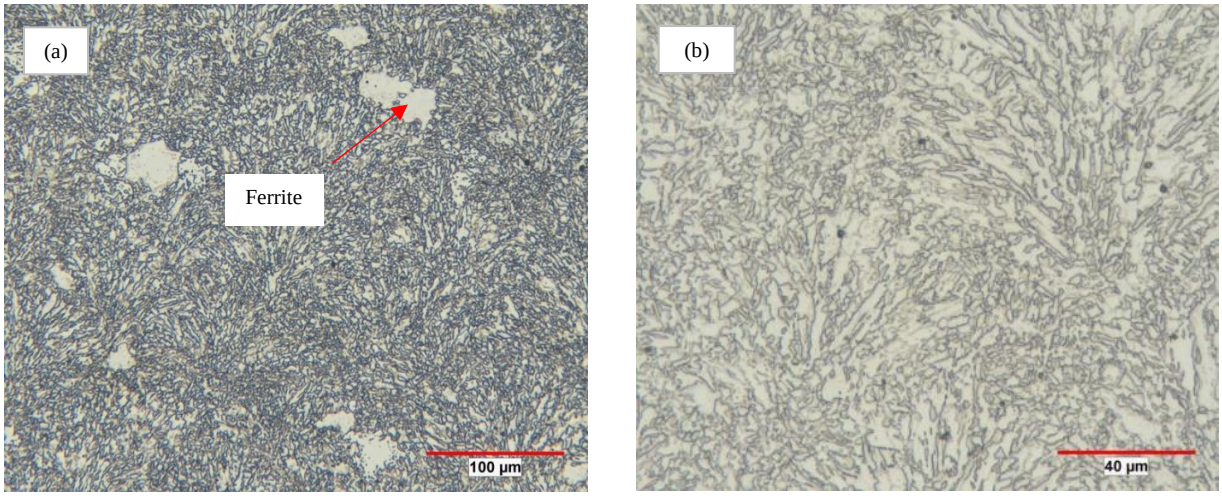

Figure 11. Etched microstructure of 816 °C WQ sample at two different magnifications.

CONCLUSIONS

- Gas atomized DP600 powder processed by LPBF achieved density comparable to wrought as well as mechanical properties using particular heat treatments.
- Dilatometry was used to measure the Ac_1 and Ac_3 transformation temperatures for LPBF samples.

- Heat treating the samples showed the wide range of strength and ductility combinations that can be achieved with one alloy.
- A difference in yield strength in compression and tension was observed after intercritically annealing samples.
- The fatigue strength of the as-built sample and the heat treated sample trended with the UTS.
- For different applications it was shown that the LPBF part's microstructure must be transformed by heat treatment to achieve the intended final properties.

REFERENCES

1. Campbell, F. C. *Elements of metallurgy and engineering alloys*. 2008, ASM International, Materials Park, Ohio.
2. C. Schade, "Processing, Microstructures and Properties of a Dual Phase Precipitation-Hardening PM Stainless Steel", 2010, Ph.D., Thesis, Drexel University, Philadelphia, PA.
3. *Standard Test Methods for Metal Powders and Powder Metallurgy Products,* 2016, Metal Powder Industries Federation, Princeton, NJ.
4. R.A. Kot and B.l. Bramfit, *Fundamentals of Dual-Phase Steels,* 1981, The Metallurgical Society of AIME, Warrendale, Pa.
5. C.R. Brooks, *Principles of the Heat Treatment of Plain Carbon and Low Alloy Steels,* 1996, ASM International, Materials Park, OH.
6. Bräutigam–Matus, K.; Altamirano, G.; Salinas, A.; Flores, A.; Goodwin, F. Experimental Determination of Continuous Cooling Transformation (CCT) Diagrams for Dual-Phase Steels from the Intercritical Temperature Range. Metals 2018, 8, 674. https://doi.org/10.3390/met8090674
7. Y. Wang, P. de Souza Ciacco, R. Ordonez, and C. Isaac Garcia, "A Comparison Study of the Austenite Grain Growth and Its Transformation Behavior during Uniform Continuous Cooling of a Wrought and Selective Laser Melting 4340 Steels," Materials Performance and Characterization 10, no. 1 (2021): 126-145. https://doi.org/10.1520/MPC20200121
8. ArcelorMittal, "Dual Phase Steels Data Sheet", March 2019 https://usa.arcelormittal.com/~/media/Files/A/Arcelormittal-USA-V2/what-we-do/price-list/2019-03-datasheet-dualphase-final.pdf